JOURNAL OF CATALYSIS 156, 65–74 (1995)

Synthesis, Characterization, and Catalytic Activity of Ti-MCM-41 Structures

T. Blasco, A. Corma,[1] M. T. Navarro, and J. Pérez Pariente

Instituto de Tecnología Química, UPV-CSIC, Universidad Politécnica de Valencia, Avenida Los Naranjos s/n, 46071 Valencia, Spain

Received January 6, 1995; revised May 18, 1995

Ti-containing MCM-41 mesoporous materials with regular 35 Å pore diameters have been obtained by direct synthesis. The OH/SiO_2 ratio and alkali metal cation content are important variables to prepare good materials. By means of IR spectroscopy, XRD, N_2 and Ar adsorption, thermal analysis, DRS-UV and EXAFS-XANES techniques, it has been shown that samples with MCM-41 structure were prepared, Ti is in framework positions and no extraframework TiO_2 was detected. The materials prepared are selective catalysts for oxidation of different types of olefins. The intrinsic activity of Ti-MCM-41 is lower than Ti-Beta and TS-1 when using H_2O_2 as oxidant. When using tertbutyl hydroperoxide the activity of Ti-MCM-41 is closer to that of Ti-Beta and much higher than for TS-1. Ti-MCM-41 has a clear advantage over the other Ti zeolites in the oxidation of large organic molecules of interest for production of fine chemicals. © 1995 Academic Press, Inc.

INTRODUCTION

The synthesis of Ti-containing zeolites has opened new possibilities for using molecular sieves as oxidation catalysts (1–10). In this way, two medium-pore zeolites, TS-1 and TS-2, with MFI and MEL structures, respectively, were shown to be active and selective catalysts for oxidation of phenol to cathecol and hydroquinone (7, 11, 12), olefins to epoxides (13, 14), and alkanes to alcohols and ketones (15–17). Recently (18), another medium-pore zeolite, Ti-ZSM-48 was synthesized but it was found not to be catalytically active, probably due to the existence of extraframework Ti species (19).

The possibilities of Ti zeolites as oxidation catalysts were expanded when a large-pore Ti-Beta zeolite was synthesized (20, 21). In this zeolite, when properly prepared, the Ti occupy framework positions, and owing to its larger pore diameter it was able to oxidize cycloalkanes, cyclohexenes, and cycloalcohols more efficiently than the TS-1 zeolite (22, 23). Meanwhile terbutyl hydroperoxide could be used as an oxygen donor, when using Ti-Beta as the oxidation catalyst.

Despite the fact the introduction of the large-pore Ti-Beta zeolite was one step forward in the preparation of zeolitic oxidation catalysts, its application is still limited to molecules smaller than 7 Å. There is no doubt that this is a limitation for the use of Ti zeolites as selective oxidation catalysts in the field of fine chemicals. There was therefore a need for producing molecular sieve oxidation catalysts with pore diameters larger than 7 Å. In a recent communication (24), we have shown the possibility of synthesizing a mesoporous Ti-MCM-41 material with the same regular hexagonal shape of the pore openings (35 Å) as in the silica-based MCM-41 material (25). The Ti-MCM-41 was shown to be catalytically active for oxidation of cyclododecene. A communication has also been presented recently (26) that shows another Ti-containing mesoporous material called Ti-HMS.

In this paper we report on the synthesis of Ti-MCM-41 materials, with and without framework Al, together with a thorough characterization of the catalysts by means of XRD, IR, UV–visible, Raman, and EXAFS-XANES spectroscopies, in order to give some insight into the coordination state of Ti in Ti-MCM-41 samples, which is crucial for proper understanding of their structure and catalytic behavior. Finally, the oxidation of reactants of different sizes shows the benefits of the ultralarge pores for performing oxidations of organic molecules, which are more sterically impeded in Ti-Beta zeolites.

EXPERIMENTAL

Synthesis

Several Ti-containing MCM-41 samples were prepared using amorphous silica (Aerosil 200, Degussa), 25 wt% aqueous solution of tetramethylammonium hydroxide (TMAOH, K + Na < 5 ppm, Alfa), an aqueous solution of hexadecyltrimethylammonium bromide (CTABr, Merck), and titanium isopropoxide (Alfa). A pure silica sample was also prepared following the procedure given in Ref.

[1] To whom correspondence should be addressed.

0021-9517/95 $12.00

TABLE 1

Chemical Composition of the Synthesis Mixtures (SiO_2 = 1) and Calcined Solid Products

	Synthesis (molar)						Solid (wt%)	
Sample	Al_2O_3	CTA	TMA	H_2O	OH	TiO_2	TiO_2	Al_2O_3
1	0	0.40	0.26	24	0.26	0	0	0
2	0	0.36	0.26	24	0.43	0.011	1.7	0
3	0	0.40	0.26	24	0.26	0.017	2.4	0
4	0	0.40	0.26	24	0.26	0.017	2.0	0
5	5×10^{-3}	0.40	0.26	24	0.26	0.017	2.2	0.83
6	0	0.45	0.26	24	0.43	0.016	2.5	0
7	0	0.36	0.26	24	0.43	0.011	1.4	0

(25). The Ti-containing samples were prepared as follows. An aqueous solution of tetramethylammonium silicate (25 wt% TMAOH 10 wt% SiO_2) was added to an aqueous solution containing 29.0 wt% hexadecyltrimethylammonium bromide. When the solution was homogenized, the silica and the titanium alkoxide were added. Aluminum was also added in one preparation (sample 5), as hydrated alumina (Catapal B, Vista, 70 wt% of Al_2O_3) before the addition of the titanium compound. Finally, in one preparation (sample 3) the titanium alcoxide was hydrolyzed in the CTABr solution, and then the other components of the reaction mixture were subsequently added. The chemical composition of the synthesis mixtures are given in Table 1.

The gels were heated in 60-ml teflon-lined stainless steel autoclaves at 408 K for 14 h under static conditions. After filtering, the solids were washed and dried at 353 K overnight. When required, the samples were heated in a flow of N_2 (150 cc min^{-1}) at 813 K for 1 h, followed by 6 h treatment in a flow of air (150 cc min^{-1}) at the same temperature.

Characterization

X-ray powder diffraction patterns were recorded using Cu$K\alpha$ radiation with a Phillips PW 1830 diffractometer equipped with a graphite monochromator. The position of the peaks was measured after dehydration of the samples for 1 h at 383 K and further rehydration over a $CaCl_2$-saturated solution (35% relative humidity) for 16 h. Si was used as the internal standard. Concentrations of Al, Ti, and alkali metal cations were determined by atomic absorption and flame emission spectroscopy. Diffuse reflectance spectra in the 190–800 nm range were recorded with a Shimadzu UV-2101 PC spectrometer equipped with a diffuse reflectance attachment using $BaSO_4$ as a reference. IR spectroscopy was carried out in a Nicolet-FTIR on KBr pellets containing 2.5 wt% sample.

The X-ray absorption spectra of the Ti-MCM-41 were acquired using Synchrotron radiation provided by the LURE (Orsay, France). The X-ray beam was emitted by the DCI storage ring running at 1.85 GeV with an average current of about 250 mA. X-rays were monochromatized using an Si(311) two-crystal monochromator. The Ti K-edge spectra were recorded at room temperature in the transmission mode. Detection was carried out by using two ion chambers, the first one (I_0) filled with He/Ne and the second one (I_1) with air below atmospheric pressure. Experimental data were analyzed with a chain of programs developed by Michalowicz (27).

The XANES spectra were treated by subtracting a linear background determined by least-square fitting of the pre-edge experimental points. The spectra were normalized with respect to the beginning of EXAFS oscillations at around 45 eV above the absorption edge, as a unit. The first inflection point of the spectrum of metallic titanium was used as the energy reference. EXAFS modultions were analyzed using standard methods.

The standard procedures for background removal, extraction of EXAFS signals, and normalization of the edge absorption were applied. The K^3 weighted Fourier Transform between 2.60 and 10.50 $Å^{-1}$ was calculated using a Kaiser window. Filtering of the first peak between 1.00 and 1.80 Å was carried out in order to analyze the first coordination shell of Ti. The EXAFS spectrum of anatase was used as a reference to calculate the phase shift function and backscattering amplitude for Ti–O (6 oxygen at a mean distance of 1.95 Å).

The spectra of the calcined dehydrated Ti-MCM-41 sample were recorded in a special chamber under vacuum. Samples were transferred in a glove box under an inert atmosphere.

The parameters fitted in the simulation were N (number of neighboring atoms), σ (Debye–Waller factor), R (distance), and ΔE_o. The electron inelastic mean free path was taken as $1/\Gamma$ with $\Gamma = 1$. The Debye–Waller factor value given in the present work ($\Delta\sigma^2$) is referred to anatase.

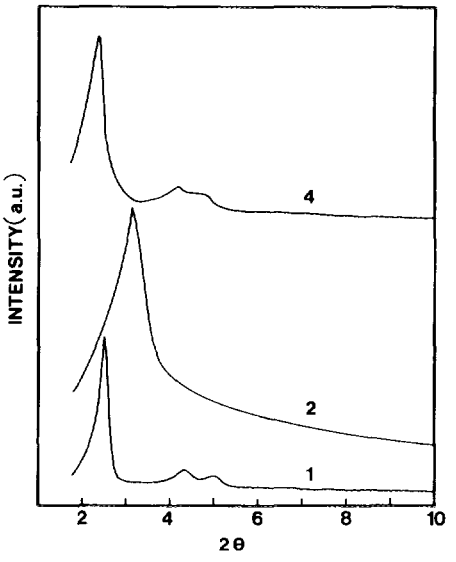

FIG. 1. XRD patterns of Ti-free (sample 1) and Ti-containing MCM-41 samples. The numbers in the figures correspond to the sample numbers in Table 1.

Catalytic Experiments

The catalytic experiments were carried out in a glass flask reflux under stirring. The flask was heated by means of a temperature-controlled oil bath, and the reaction mixture was magnetically stirred. Aliquots were taken at selected reaction times. The products were separated and analyzed by gas chromatography in a capillary column (5% methylphenylsilicone, 25 m in length), and an FID detector identification of the different products was done by GC-MS and available reference standards. H_2O_2 and terbutyl hydroperoxide (TBHP) were used as oxygen donors.

RESULTS AND DISCUSSION

Synthesis

The synthesis of Ti-MCM-41 has been carried out in the absence of alkali cations since they usually promote the formation of poor crystalline titanosilicates during the synthesis of TS-1 and β-zeolites (21). Under these conditions, an optimum OH/SiO_2 ratio equal to 0.26 has been found, the other compositional parameters remaining unchanged (Table 1). Higher ratios result in less crystalline materials, with ill-defined XRD patterns (Fig. 1, sample 2). Ti-MCM-41 can also be prepared in the presence of aluminum, this element being found in the crystalline product recovered after gel autoclaving (Table 1). For Si/Al = 100 in the starting mixture, a negligible influence of aluminum in the quality of the product is observed (Tables 2 and 3).

The most intense peaks of the crystalline materials can be indexed in a hexagonal unit cell, with values of the cell parameter a_0 close to the titanium-free sample (Table 2).

TABLE 2

XRD d_{100} Peak and Hexagonal Unit Cell Parameter a_0

	As-synthesized		Calcined	
Sample	d_{100} (Å)	a_0 (Å)[1]	d_{100} (Å)	a_0 (Å)
1	38.8	44.8	34.9	40.3
2	35.1	40.5	28.4	32.8
3	36.5	42.1	33.0	38.1
4	38.7	44.7	37.8	43.6
5	39.7	45.8	37.8	43.6
6	34.5	39.8	28.1	32.4
7	36.57	42.2	28.8	33.2

A cell contraction of 2–4 Å upon calcination is observed in Ti-MCM-41 (Table 2), a phenomenum already reported for Ti-free MCM-41 (25).

At present, no clear influence of the Ti content on the unit cell parameter has been demonstrated. Indeed, the d_{100} values are very sensitive to the degree of organization of the product (Table 2, samples 2 and 4). In this way, the hypothetical variation of the cell parameter cannot be used as a proof to ascertain the incorporation of Ti into the framework, as is the case with Ti-containing zeolites (11). However, it can be noticed that the a_0 value of good crystalline Ti-MCM-41 is 2–4 Å higher than the pure siliceous material. Beck *et al.* (25) have reported a_0 values of aluminum-containing MCM-41 higher than the pure siliceous counterparts. This could be an indication that the titanium has been incorporated into the tetrahedral network.

N_2 and Ar Adsorption

Figure 2 shows the N_2 adsorption–desorption isotherms of samples 1 and 4, which can be taken as representatives of the other samples. The inflection in the adsorption isotherm at P/P_0 = 0.2–0.3 indicates the mesopore filling.

TABLE 3

Pore Diameter and Volume Determined by Ar Physisorption and BET Area

	Ar		
Sample	V_p (cm^3 g^{-1})	Pore size (Å)	BET area (m^2 g^{-1})
1	0.17	—	794
2	—	—	881
3	0.45	31	884
4	0.70	35	1102
5	0.66	35	1060
6	0.28	20	725
7	0.25	20	589

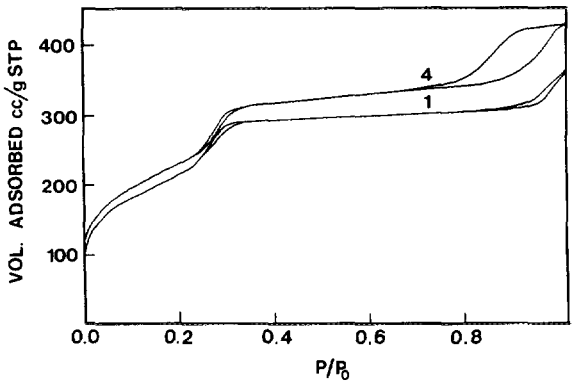

FIG. 2. N_2 adsorption/desorption isotherms of Ti-free (sample 1) and Ti-containing MCM-41 sample 4. The numbers in the figures correspond to the sample numbers in Table 1.

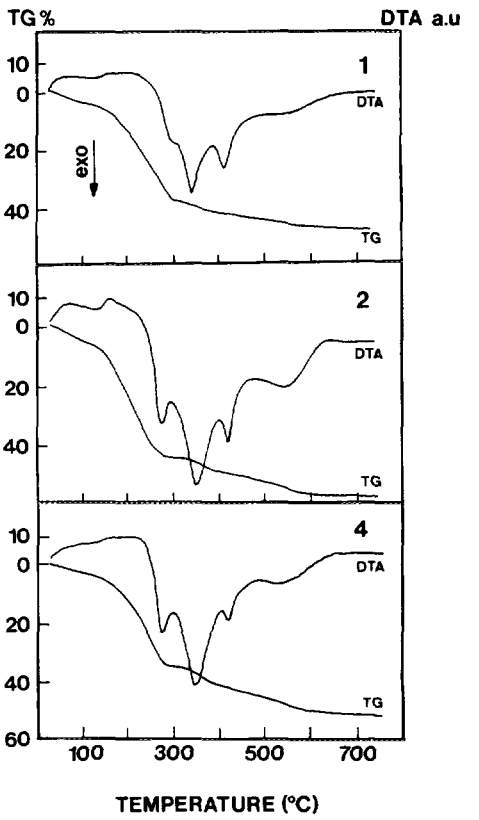

FIG. 3. TGA-DTA traces of as-synthesized Ti-free (sample 1) and Ti-containing MCM-41 samples. The numbers in the figures correspond to the sample numbers in Table 1.

BET areas close to 900 $m^2\ g^{-1}$ (Table 3), even for the poorly crystalline sample 2, were found. The average pore diameters and pore volumes ≤70 Å obtained from the method of Horvath and Kawazoe (28) applied to the Ar adsorption isotherms are also given in Table 3. From the difference between the Ar pore diameters and a_o values given in Table 2, the wall thickness between pores can be estimated to be ~7–9 Å, similar to the values already reported for Ti-free MCM-41 (29). The wall thickness can eventually become an important parameter in determining the catalytic behavior of Ti-MCM-41. Indeed, if we assume an average $T \cdots T$ (T = Si or Ti) distance of ~3.0 Å, the wall between channels should be constructed by no fewer than three tetrahedral TO_4, which could belong to edge-sharing 3-, 4-, or 5-membered rings of the tetrahedra. Two of the tetrahedra should be accessible from the channels, but the inner one would be eventually "shielded" in the silicon core of the wall, following the model proposed by Davis *et al.* (30). This inner tetrahedral position should probably remain inaccessible from the channels, rendering potentially inactive any titanium atom located in these positions.

Thermal Analysis

Thermogravimetric (t.g.) and differential thermal analysis (d.t.a.) of the pure silica sample and two Ti-containing materials, samples 2 and 4, are given in Fig. 3. The thermal patterns of the three samples are qualitatively very similar. The total weight losses are 49.2, 59.4, and 51.0 wt% for samples 1, 2, and 4, respectively. Three distinct steps can be distinguished; 25–130°C, 130–300°C, and above 300°C. The first step is due to the desorption of water. The two other weight losses are associated to exothermic processes related to the combustion of the organic species. It can be noticed that the weight losses of both Ti-MCM-41 samples are similar, which indicates a similar pore filling, despite the less-defined XRD pattern of sample 2. This is an indication that the channels of the as-synthesized sample 2 should be similar in size to the ones present in the high-crystalline sample 4.

IR Spectroscopy

The IR spectra of Ti-MCM-41 samples are given in Fig. 4. The spectra closely resemble that of Ti-free MCM-41 (sample 1), and a band at 960 cm^{-1} is clearly visible in all spectra. For pure silicate or aluminosilicate materials this band has been assigned to the Si–O stretching vibrations of $Si–O^-\ R^+$ groups, as $R^+ = H^+$ in the calcined state (31). The strong intensity of this band in the pure siliceous MCM-41 is due to the great amount of silanol groups present in the calcined material (32). For Ti-containing zeolites, a band at 960 cm^{-1} increasing in intensity with the Ti content is generally taken as a proof of the incorporation of this metal into the framework (33). Obviously, in the case of Ti-MCM-41, this criteria can not be used to ascertain the incorporation of the metal into the structure, and other techniques should be used to prove this.

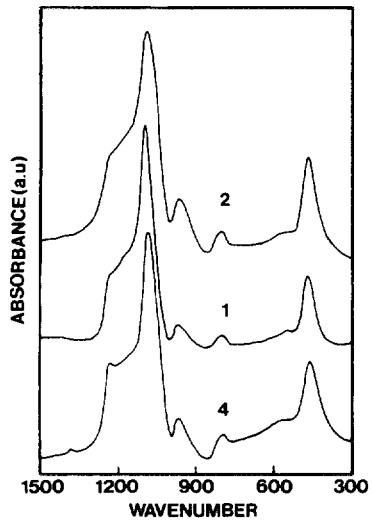

FIG. 4. IR spectra in the framework vibration region of Ti-free and Ti-containing MCM-41 samples. The numbers in the figures correspond to the sample numbers in Table 1.

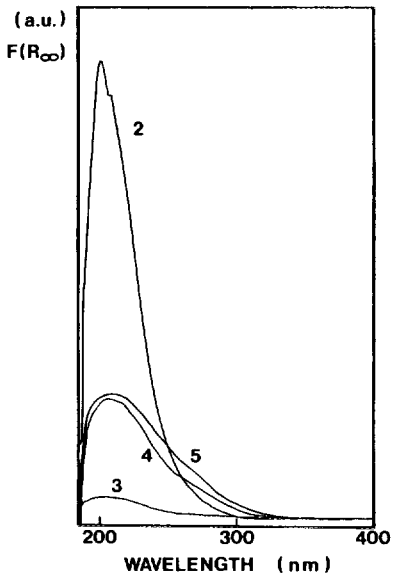

FIG. 5. Diffuse reflectance UV–visible spectra of different Ti-MCM-41 samples. The numbers in the figures correspond to the sample numbers in Table 1.

UV–Visible Diffuse Reflectance

DR-UV spectroscopy is a very sensitive probe for the presence of extraframework Ti in zeolites. We have characterized the Ti-MCM-41 samples by DR-UV and the spectra of calcined samples are given in Fig. 5. An intense band centered at ca. 215 ± 5 nm is observed in the spectra, as well as a shoulder at ~270 nm, which is absent in sample 2. No other spectral features appear, and the absence of a band at ~330 nm indicates that anatase is not present in significant amounts in the crystals. The shoulder at 270 nm probably corresponds to partially polymerized hexacoordinated Ti species (34) and its absence in sample 2 could be a consequence of its lower Ti content.

An intense band at ca. 220 nm is also present in TS-1 (34) and Ti-Beta (20), and has been assigned to the ligand-to-metal charge transfer (CT) involving isolated Ti atoms in octahedral coordination, in which two water molecules form part of the metal coordination sphere. According to this assignment, the band at ca. 215 ± 5 in Ti-MCM-41 should be due to isolated Ti(IV) in an octahedral environment. It can be noted that the intensity of this band in sample 3, obtained from a gel in which the titanium alcoxide was first hydrolyzed in a CTABr solution (slightly acidic medium), is much lower than in the other samples, despite their similar metal content. The reason for this is not yet clear to us, but it suggests that the Ti environment could be different in this sample.

It can be also remarked that sample 2, despite having a less-defined XRD pattern, still shows the Ti to be in framework positions according to its DR spectrum, and no extraframework titanium species are detected (Fig. 5).

TABLE 4

Pre-edge Peak Parameters for Ti Reference Compounds

Compound	Ti site symmetry	[a]Peak position (±0.2 eV) $A_1/A_2/A_3$	Intensity (height) ±5%	[b]FWHM (±0.2 eV)	Reference
Ba_2TiO_4	Tetrahedral	3.5	0.84	1.5	(55)
Fresnoite	Square pyramidal	4	0.60	_	(39)
Ramasayite	Very distorted Octahedral	2.8/4.8/8.5	0.08/0.29/0.13	_	(22)
Anatase	Distorted octahedral	2.5/5.5/8.0	0.04/0.21/0.21	_	(22)

[a] Relative to the first inflection point for Ti metal.
[b] The full width at half maximum.

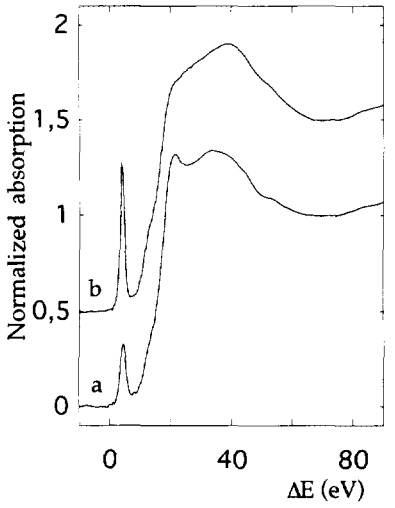

FIG. 6. Ti K-edge XANES spectra of Ti-MCM-41 sample 2, (a) calcined and (b) calcined and dehydrated.

X-Ray Absorption

Comparison of the pre-edge features appearing in XANES spectra with model compounds provides information about the symmetry environment of the scattering atom. Previous studies on reference compounds have shown that octahedral Ti, as in anatase and rutile, gives rise to three prepeaks usually denoted A_1, A_2, and A_3 (35). The characteristics of the anatase prepeaks are shown in Table 4. A_2 and A_3 have been attributed to the 1*s* to t_{2g} and e_g elecronic transitions, respectively, while the origin of A_1 is still controversial (35–37). The intensity of the central peak increases with increased site distortion owing to the relaxation of the inversion symmetry around Ti (37–39), and it is the only one detected for very distorted octahedral sites. A single and intense pre-edge feature is observed in tetra- and pentacoordinated Ti compounds because of the lack of inversion symmetry (37–39), as can be seen in Table 4 for fresnoite and Ba_2TiO_4 with fivefold and fourfold coordinated Ti, respectively. The environment around Ti also affects the position of the main pre-edge feature (peak A_2), which is shifted to lower energy with decreased coordination (see Table 4). On the other hand, Waychunas (38) observed that the A_2 peak appears at lower energy in titanosilicates than in Ti oxides, as can be observed comparing anatase and ramsayite in Table 4.

Figure 6 shows the XANES spectra of sample 2 calcined, and calcined and dehydrated. A dramatic change in the pre-edge features is observed after dehydration, indicating a modification in the site symmetry of Ti atoms. The characteristics of the prepeaks are shown in Table 5. The prepeak intensity in the calcined material suggests a distorted octahedral environment for Ti, as can be deduced from comparison with model compounds in Table 4. The energy

TABLE 5

Ti Pre-edge Peak Parameters for Sample 2

Compound	[a]Peak position (±0.2 eV) $A_1/A_2/A_3$	Intensity (height) ±5%	[b]FWHM (±0.2 eV)
Calcined	4.2	0.33	2.0
Calcined dehydrated	3.8	0.77	1.2

[a] Relative to the first inflection point for Ti metal.
[b] The full width at half maximum.

position is shifted with respect to Ti oxides and within the range of titanosilicates minerals (38) (see ramsayite and anatase in Table 4). Recently, Pei *et al.* (40) claimed that Ti is tetrahedrally coordinated in calcined TS-1 stored at ambient conditions before recording the spectra. However, previous studies on Ti-substituted TS-1 (39, 41–44), TS-2 (45, 46), Ti-Beta (22), and TS-48 (47), in the calcined state, have shown the existence of various Ti sites. Although it will also be probably true for sample 2, the pre-edge characteristics, i.e., energy position and intensity, suggest mainly octahedral coordination for Ti, as it has been also reported for TS-1 in certain synthesis conditions (42).

Upon dehydration, a sharper and more intense prepeak at lower energy is observed in the XANES spectrum, indicating a decrease in the coordination of Ti. This same effect has been observed for TS-1 (42, 44) and Ti-Beta (22) and attributed, with the support of EXAFS data, to an evolution of the Ti site symmetry towards tetrahedral, suggesting that Ti has effectively been incorporated into the framework. The lower intensity for sample 2, with respect to Ba_2TiO_4, may be due either to the presence of small amounts of Ti in higher coordination or to a slightly different Ti site symmetry.

In order to obtain further insight into the coordination

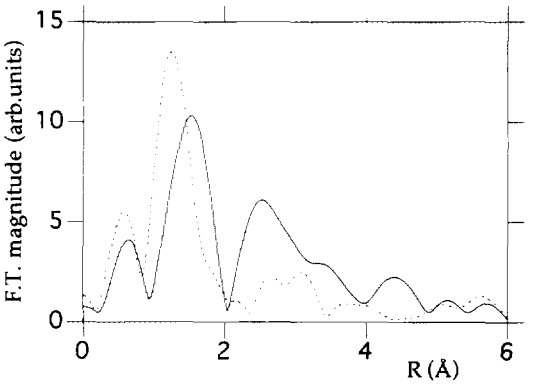

FIG. 7. Fourier transform magnitude of the K^3-weighted EXAFS signals of anatase (solid line) and calcined, dehydrated Ti-MCM-41 sample 2 (dashed line).

TABLE 6

EXAFS Simulation Parameter for the First Shell of Calcined Dehydrated Sample 2.

Neighbor	N (±0.5)	R(Å)	$\Delta\sigma^2$ (Å^2)	ΔE_0 (eV)	Fit value
Oxygen	4.3	1.81 ± 0.02	4×10^{-4}	0.8	5×10^{-3}

environment of Ti, we carried out the analysis of the EXAFS data of the calcined and dehydrated sample 2. Figure 7 shows the radial distribution functions of sample 2 and anatase without phase correction. The maximum of the first peak, corresponding to the first coordination shell around Ti appears at 1.2 Å in sample 2 and 1.5 Å in anatase (without phase correction), suggesting a lower Ti–O average distance for the former. Table 6 shows the best set of parameters found in the simulation of the first shell using the Ti–O phase shift and backscattering functions from anatase, while the experimental and simulated oscillations are shown in Fig. 8. The average Ti–O distance in sixfold coordinated silicates is between 1.94 Å (48) and ca. 2.06 Å (49). In fresnoite, with fivefold coordinated Ti the mean Ti–O distance is 1.92 Å (50). The only crystalline model compound with tetrahedrally coordinated Ti is Ba_2TiO_4 with an average Ti–O distance of 1.81 Å (51). Dumas *et al.* (52) found a Ti–O bond length of 1.85 Å for tetrahedral Ti in TiO_2–SiO_2 glasses. The reported average Ti–O distance for fourfold coordinated Ti in TS-1, TS-2, and Ti-Beta are in the range 1.80–1.88 Å (22, 40–46). Both the coordination number and the Ti–O distance for calcined dehydrated sample 2 (Table 6) indicate tetrahedral coordination for Ti, in good agreement with the above-discussed XANES results.

Analysis of the second coordination shell of Ti in calcined TS-1 (41) and calcined dehydrated Ti-Beta (22) revealed the presence of Si atoms, supporting the Ti incorporation into substitutional framework positions. Trong On and co-workers carried out a multishell analysis on TS-1 (43) and TS-2 (45–46) and found very short Ti–Si distances ca. 2.2–2.4 Å. This result led to the authors to propose a model where Ti atoms are not isomorphously substituted for silicon, but are linked to the framework by an edge-sharing type of linkage. Recently, Pei *et al.* (40) analyzed the second peak in the FT spectrum of TS-1 and concluded that it consisted of at least two subshells which should contain O and/or Si at distances between 3.1 and 3.8 Å. In this latter publication (40), the authors disagree with the interpretation made by Trong On and co-workers (45, 46) of the FT spectrum and report that they do not find any evidence for the existence of the edge-sharing Ti species. They conclude that Ti is tetrahedrally coordinated, occupying framework positions. Figure 7 shows that the second peak in the FT spectrum of sample 2 appears to be split and appears at higher R values than anatase, suggesting that it does not correspond to the presence of extraframework oxidic phases. We tried to simulate the filtered signal of the second shell with the use of Ti–Si, Ti–Ti, and Ti–O amplitude and phase functions calculated by Mckale (53) without any success. It was only possible to partially fit the EXAFS oscillations for $K > 6$ Å^{-1} with Ti–Si functions at a distance of 3.15 Å. However, we are not able to fit the whole K range, even with the use of several subshells. Thus, we cannot assess the presence of Si atoms at a distance of ca. 3.15 Å, although this is within the expected range for Ti–O–Si bonds in a tridimensional [SiO_4]-based framework. The difficulties in the simulation of the second shell in sample 2 may arise in part from the low Ti content in the sample, which makes the spectrum noisy. However, the principal factor will probably be the large variety of distances expected in the disordered inorganic portion of the material, which would increase the Debye–Waller factor.

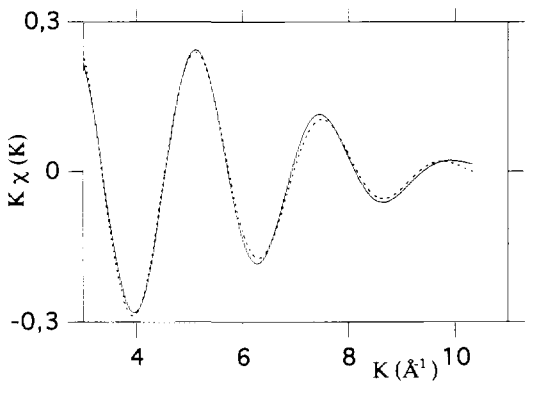

FIG. 8. Comparison between the experimental (solid line) and calculated data (dashed line) obtained in the simulation of the first coordination shell around Ti in the calcined, dehydrated Ti-MCM-41 sample 2.

Catalytic Results

It has been shown above that the different physicochemical techniques indicate that in the Ti-MCM-41 samples prepared, the Ti is in framework positions, and therefore it could be active for carrying out catalytic oxidations of hydrocarbons using peroxides as oxidants. Here we have

TABLE 7

Activity of Ti-Zeolites for Oxidation of 1-Hexene with H_2O_2

Catalyst sample	Ti content (wt% TiO_2)	Alkene conversion (mol% of max)	Turnover (mol/mol Ti)	Epoxide selectivity (mol%)	H_2O_2 selectivity (%)
Euro TS-1	3.8	48.8	98	96	99
Ti-Beta	3.2	38.4	33	7	94
Ti-MCM-41	2.5	9.1	4	96	65

Note. (35 wt.%), 323 K, 1 h, and 0.20 g for Euro TS-1 and Ti-Beta, and 0.60 g catalyst for Ti-MCM-41 (sample 6).

carried out the oxidation of different types of olefins on Ti-MCM-41 samples and the results are compared with those obtained with the large-pore Ti-Beta and the medium-pore Euro TS-1 zeolites. First, the oxidation of a small molecule such as *n*-hexene, which can easily diffuse in any of the three structures, was performed in order to compare the intrinsic activity of the catalysts. The results given in Table 7 clearly show that the intrinsic activity is Euro TS-1 > Ti-Beta > Ti-MCM-41. This indicates that even though the coordination of Ti is similar in the three cases, and most of the Ti atoms are in an Si reach environment, the redox potential and/or the adsorption characteristics of the samples are different, showing a different final reactivity. On top of that, we can not reject the possibility that in Ti-MCM-41 samples, some of this Ti is located in the "shielded" core of the wall and remains unaccessible from the channels.

The Euro TS-1 and Ti-MCM-41 are much more selective toward the formation of epoxide than Ti-Beta, as a consequence of the presence of Brønsted acid sites associated to framework Al which are present in the latter zeolite and are responsible for the opening of the epoxide ring to form glycol and ethers. A lower selectivity on H_2O_2 has been observed on Ti-MCM-41 than on either Euro TS-1 or Ti-Beta.

It should be taken into account that, as has been observed by EXAFS, H_2O has a strong tendency to coordinate with the four coordinated Ti species. Then H_2O, when present, will compete with the reactant which also has to be adsorbed on the Ti atom in the transition state. Thus, it appears that the water concentration and the hydrophobic-hydrophilic characteristics of the samples are going to be of great importance for the global catalytic phenomena. In the case of the three zeolites compared here, it is clear that if one takes into account the large population of silanol groups present in calcined MCM-41 samples (54) the order of hydrophobicity should be Euro TS-1 > Ti-Beta > Ti-MCM-41. If this is so, one could expect a lower activity and lower H_2O_2 selectivity for the Ti-MCM-41 sample, as it is observed experimentally. However, the behavior could be different if the reaction is carried out in a water-free reaction media. Then, when the 1-hexene oxidation was carried out using terbutyl hydroperoxide (TBHP) as oxidant, not only is a very high selectivity for TBHP obtained but the activity of the Ti-Beta and Ti-MCM-41 are now closer (Table 8). Owing to the size of TBHP, the activity of the Euro TS-1 was very small when the reaction was carried out with this oxidant, and therefore it is not considered in Table 8.

In the case of MCM-41 materials, it is known (25) that the wall of the pores are amorphous. Then, it is of interest to compare the oxidation behavior of Ti-MCM-41 with an amorphous Ti–SiO_2 catalyst (Grace Ti-modified silica gel with 0.28% TiO_2 with 328 $m^2 g^{-1}$). Thus, we have performed the oxidation of 1-hexene on the Ti–SiO_2 sample under the experimental conditions reported in Tables 7 and 8. The Ti–SiO_2 sample was inactive when H_2O_2 was used as oxidant, while in the case of TBHP a conversion of 0.8%

TABLE 8

Activity of Ti Catalysts for Oxidation of 1-Hexene with TBHP

Catalyst sample	Ti content (wt% TiO_2)	Alkene conversion (mol% of max)	Turnover (mol/mol Ti)	Epoxide selectivity (mol%)
Ti-Beta	3.2	10.2	42	100
Ti-MCM-41	2.5	6.3	17	100

Note. Reaction conditions: 50 mmol alkene, 60 mmol TBHP, 333 K, 8 h, 0.30 g Ti-Beta, and 0.60 g of Ti-MCM-41 (sample 6).

TABLE 9

Oxidation of α-Terpineol on Ti Catalysts using TBHP

Catalyst sample	Ti content (wt% TiO_2)	Reaction time (h)	Alkene conversion (mol%)	Cineol (mol%)	Epoxide (mol%)
Ti-Beta	3.2	9	24.1	14.1	10.0
		24	32.7	19.9	12.8
Ti-MCM-41	2.0	9	44.6	23.1	21.5
Sample 4		24	62.2	32.0	30.2

Note. Reaction conditions: 1.00 mmol α-terpineol, 1.10 mmol TBHP, 10 ml acetonitrile, 20 wt% catalyst, and 353 K reaction temperature.

TABLE 10

Activity of Ti-MCM-41 for Oxidation of Ciclohexene with TBHP

Ti-MCM-41 samples	Ti content (wt% TiO_2)	Alkene conversion (mol% of max)	Epoxide selectivity (mol%)
Sample 2	1.7	14.1	93
Sample 4	2.0	13.5	90

Note. Reaction conditions: 56.3 mmol of alkene, 14.0 mmol TBHP, 333 K, 5 h reaction time, and 0.3 g catalyst.

was observed after 8 h, instead of 6.3% in the case of Ti-MCM-41. However, when the activity per Ti atom (turnover) was calculated the values obtained are practically the same for Ti-MCM-41 and Ti–SiO_2. This would indicate that the Ti species must be quite similar on these two types of materials. One may expect, howver, that for larger Ti contents, as in the order of the Ti-MCM-41 sample, the turnover on the Ti–silica will be smaller, probably due to the formation of Ti–O–Ti bonds.

The benefit of using the mesoporous Ti-MCM-41 sample instead of zeolites could be seen when large organic molecules are to be oxidized. Indeed, the results from Table 9 clearly show that α-terpineol is oxidized more rapidly on Ti-MCM-41 than on Ti-Beta.

Finally, and in order to see if samples 2 and 4, which show differences in crystallinity, gave different activities and/or selectivities, cyclohexene was oxidized using TBHP as oxidant. The results from Table 10 indicate that the activity and selectivity of these two catalysts are very similar, in agreement with the DR-UV spectroscopy which showed a similar spectra for samples 2 and 4, and indicate that the Ti was present in framework positions, and no extraframework titanium species were detected in any of the two samples.

CONCLUSIONS

A mesoporous material with a MCM-41 structure has been synthesized containing Ti and Si in the framework. It has been found that the optimum OH/SiO_2 ratio for the preparation of good crystalline materials is 0.26, provided the other compositional parameters remain unchanged.

Ti-MCM-41 samples can also been prepared with tetrahedral Al, combining oxidation and acid sites.

The different characterization techniques show that Ti is in the framework in Si-rich environments. In the hydrated form isolated Ti atoms exist in octahedral coordination in which two water molecules form part of the metal coordination sphere.

Upon dehydration an evolution of the Ti site symmetry toward tetrahedral was observed.

Ti-MCM-41 samples show a lower intrinsic activity and lower selectivity toward the use of H_2O_2 for olefin oxidation than either Ti-Beta or Ti–silicalite. However the Ti-MCM-41 prepared in the absence of Al shows a high selectivity for formation of epoxides.

Owing to their high hydrophilicity Ti-MCM-41 samples present a good catalytic behavior for oxidations in water-free media, when using organic peroxides as oxidants. Under these circumstances its catalytic behavior approaches that of Ti-Beta.

For the oxidation of larger organic molecules, such as α-terpineol, which are diffusion-limited even in a large-pore zeolite such as Ti-Beta, the mesoporous Ti-MCM-41 catalyst gives much better results than the above zeolites, and opens new possibilities for the production of oxygenated fine chemicals.

ACKNOWLEDGMENTS

Financial support by CICYT (MAT 94-0359-C02-01) is gratefully acknowledged.

REFERENCES

1. Perego, G., Bellussi, G., Como, C., Taramasso, M., Buonomo, F., and Esposito, A., *Stud. Surf. Sci. Catal.* **28,** 129 (1986).
2. Tuel, A., and Ben Taarit, Y., *Zeolites* **13,** 357 (1993); Tuel, A., and Ben Taarit, Y., *Microporous Mater.* **1,** 179 (1993); Tuel, A., and Ben Taarit, Y., *Zeolites* **14,** 272 (1994).
3. Tatsumi, T., Nakamura, M., Negishi, S., and Tominages, M., *J. Chem. Soc. Chem. Commun.*, 476 (1990).
4. Huybrechts, D. R. C., De Bruycker, L., and Jacobs, P. A., *Nature* **345,** 240 (190).
5. Clerici, M. G., *Appl. Catal.* **68,** 249 (1991).
6. Taramasso, M., Perego, G., and Notari, B., US Patent 4,410,501 (1983).
7. Reddy, J. S., Kumar, R., and Ratnasamy, P., *Appl. Catal.* **58,** L1 (1990).
8. Bellussi, G., Giusti, A., Esposito, A., and Buonomo, F., European Patent Appl. 77522 (1982).
9. Bellusi, G., Clerici, M. G., Giusti, A., and Buonomo, F., European Patent Appl. 226258 (1988).

10. Bellussi, G., Clerici, M. G., Carati, A., and Esposito, A., European Patent Appl. 226825 (1988).
11. Thangaraj, A., Kumar, R., Mirajkar, S. P., and Ratnasamy, P., *J. Catal.* **130,** 1 (1990).
12. Romano, U., Esposito, A., Maspero, F., and Neri, C., *in* "Proceedings International Symposium on New Developments in Selectivive Oxidations, Rimini, 1989" (G. Centi and F. Trifiró, Eds.), Preprints B1.
13. Clerici, M. G., Bellussi, G., and Romano, U., *J. Catal.* **129,** 1 (1991).
14. Khouw, C. B., Dartt, C. B., Li, X., and Davis, M. E., "Symposium on New Catalytic Chemistry Utilizing Molecular Sieves, 206th National Meeting, American Chemical Society, Chicago, 1993.
15. Huybrechts, D. R. C., Buskens, Ph. L., and Jacobs, P. A., *Stud. Surf. Sci. Catal.* **72,** 21–31.
16. Clerici, M. G., Bartolomeo, A., and Bellussi, G., European Patent Appl. 412596 (1991).
17. Sudhakar Reddy, J., and Sivasanker, S., *Catal. Lett.* **11,** 241 (1991).
18. Serrano, D. P., Li, H-X., and Davis, M. E., *J. Chem. Soc. Chem. Commun.*, 745 (1992).
19. Reddy, K. M., Kaliaguine, S., Sayari, A., Ramaswamy, A. V., Reddy, V. S., and Bonneviot, L., *Catal. Lett.* **23,** 175 (1994).
20. Camblor, M. A., Corma, A., and Martínez, A., *J. Chem. Soc. Chem. Commun.*, 589 (1992).
21. Camblor, M. A., Corma, A., and Pérez-Pariente, J., *Zeolites* **13,** 82 (1993).
22. Blasco, T., Camblor, M. A., Corma, A., and Pérez-Pariente, J., *J. Am. Chem. Soc.* **115,** 11806 (1993).
23. Corma, A., Camblor, M. A., Esteve, P., Martínez, A., and Pérez-Pariente, J., *J. Catal.* **145,** 151 (1994).
24. Corma, A., Navarro, M. T., and Pérez-Pariente, J., *J. Chem. Soc. Chem. Commun.*, 147 (1994).
25. Kresge, C. T., Leonowicz, M. E., Roth, W. J., Vartuli, J. C., and Beck, J. S., *Nature* **359,** 710 (1992); *J. Am. Chem. Soc.* **114,** 10834 (1992).
26. Tanev, P. T., Chibwe, M., and Pinnavaia, T. J., *Nature* **368,** 321 (1994).
27. Michalowicz, in "Structure Fines D'Absorption X en Chimie" (M. Dexpert, A. Michalowicz, and M. Verdaguer, Eds.), Vol. 3. Ecole du CNRS, Garchy, 1988.
28. Horvath, G., and Kawazoe, K., *J. Chem. Eng. Jpn.* **16,** 470 (1983).
29. Chen, C. Y., Li, H. X., and Davis, M. E., *Microporous Mater.* **2,** 17 (1993).
30. Chen, C. Y., Burkett, S. L., Li, H-X., and Davis, M. E., *Microporous Mater.* **2,** 27 (1993).
31. Decottiguies, M., Phalippou, J., and Zarzycki, J., *J. Mater. Sci.* **13,** 2605 (1978).
32. Kolodziejski, W., Corma, A., Navarro, M. T., Pérez-Pariente, J., *Solid State Nucl. Magn. Reson.* **2,** 253 (1993).
33. Boccuti, M. R., Rao, K. M., Zecchina, A., Leofanti, G., and Petrini, G., *Stud. Surf. Sci. Catal.* **48,** 133 (1989).
34. Petrini, G., Cesana, A., De Alberti, G., Genoni, F., Leofanti, G., Padovan, M., Paparatto, G., and Rofia, P., *Stud. Surf. Sci. Catal.* **68,** 761 (1991).
35. Poumelec, B., Lagnel, F., Marucco, J. F., and Touzelin, B., *Phys. Status Solidi B* **133,** 371 (1986).
36. Poumelec, B., Marucco, J. F., and Touzelin, B., *Phys. Status Solidi B* **137,** 519 (1986).
37. Greegor, R. B., Lytle, F. W., Sandstrom, D. R., Wong, J., and Schultz, P., *J. Non-Cryst. Solids* **55,** 27 (1983).
38. Waychunas, G. A., *Am. Mineral* **72,** 89 (1987).
39. Behrens, P., Felsche, J., Vetter, S., Schultz-Ekloff, G., Jaeger, N. I., and Niemann, W., *J. Chem. Soc. Chem. Commun.*, 678 (1991).
40. Pei, S., Zajac, G. W., Kaduk, J. A., Faber, J., Boyanov, B. I., Duck, D., Fazzini, D., Morrison, T. I., and Yang, D. S., *Catal. Lett.* **21,** 333 (1993).
41. Schultz, E., Ferrini, C., and Prins, R., *Catal. Lett.* **14,** 221 (1992).
42. Lopez, A., Kessler, H., Guth, J. L., Tuilier, M. H., and Popa, J. M., "Proceedings, 6th International Conference on X-Ray Absorption Fine Structure." Ellis Horwood/Wiley, Chichester/New York, 1991.
43. Bonneviot, L., Trong On, D., and Lopez, A., *J. Chem. Soc. Chem. Commun.*, 685 (1993).
44. Bordiga, S., Boscherini, F., Coluccia, S., Genoni, F., Lamberti, C., Leofanti, G., Marchese, L., Petrini, G., Vlaic, G., and Zecchina, A., *Catal. Lett.* **26,** 195 (1994).
45. Trong On, D., Bonneviot, L., Bittar, A., Sayari, A., Kaliaguine, S., *J. Mol. Catal.* **74,** 233 (1992).
46. Trong On, D. Bittar, A., Sayari, A., Kaliaguine, S., and Bonneviot, L., *Catal. Lett.* **16,** 85 (1992).
47. Reddy, K. M., Kaliaguine, S., Sayari, A., Ramaswamy, A. V., Reddy, V. S., and Bonneviot, L., *Catal. Lett.* **23,** 175 (1994).
48. Fischer, K., *Z. Kristallogr.* **129,** 222 (1969).
49. Canillo, E., Mazzi, F., and Rossi, G., *Acta Crystallogr.* **21,** 200 (1966).
50. Moore, P. B., and Louisnathan, S. J., *Z. Kristallogr.* **130,** 438 (1969).
51. Wu, K. K., and Brown, I. D., *Acta Crystallogr. Sect. B* **29,** 2009 (1973).
52. Dumas, T., and Petiau, J., *J. Non-Cryst. Solids* **81,** 201 (1986).
53. McKale, A. G., Veal, B. W., Paulikas, A. P., Chan, S.-K., and Knapp, G. S., *J. Am. Chem. Soc.* **110,** 3763 (1988).
54. Corma, A., Fornés, V., Navarro, M. T., and Pérez-Pariente, J., *J. Catal.* **148,** 569 (1994).
55. Yarker, C. A., Johnson, P. A., Wright, A. C., Wong, J., Greegos, R. B., Lytle, F. W., Sinclair, R. N., *J. Non-Cryst Solids* **79,** 117 (1986).